1-1-2005

Phase Transition in Single Crystal Cs$_2$Nb$_4$O$_{11}$

Jianjun Liu
University of Nebraska, Omaha, Nebraska

E. P. Kharitonova
Moscow State University, Leninskiye gory, 119992 Moscow, Russia

Chun-Gang Duan
University of Nebraska, Omaha, Nebraska

W. N. Mei
University of Nebraska, Omaha, Nebraska

R. W. Smith
University of Nebraska, Omaha, Nebraska

See next page for additional authors

Authors

Jianjun Liu, E. P. Kharitonova, Chun-Gang Duan, W. N. Mei, R. W. Smith, and John R. Hardy

Phase transition in single crystal $Cs_2Nb_4O_{11}$

Jianjun Liu[a)]
Department of Physics, University of Nebraska, Omaha, Nebraska 68182-0266 and Department of Physics and Center for Electro-Optics, University of Nebraska, Lincoln, Nebraska 68588-0111

E. P. Kharitonova
Department of Physics, Moscow State University, Leninskiye gory, 119992 Moscow, Russia

Chun-Gang Duan and W. N. Mei
Department of Physics, University of Nebraska, Omaha, Nebraska 68182-0266

R. W. Smith
Department of Chemistry, University of Nebraska, Omaha, Nebraska 68182-0109

J. R. Hardy
Department of Physics and Center for Electro-Optics, University of Nebraska, Lincoln, Nebraska 68588-0111

We studied temperature dependence of complex capacitance, impedance, and polarized Raman spectra of single crystal $Cs_2Nb_4O_{11}$. First, we observed a sharp λ-shaped peak at 165 °C in the complex capacitance, then found drastic changes in the Raman spectra in the same temperature range. Utilizing the pseudosymmetry search of structure space group, we attributed the observed anomalies to a structural change from the room temperature orthorhombic *Pnn*2 to another orthorhombic *Imm*2. We also measured room temperature polarized Raman spectra in different symmetries of normal vibrations and assigned high wavenumber Raman bands to the internal vibrations of NbO_6 octahedra and NbO_4 tetrahedra. © *2005 American Institute of Physics.* [DOI: 10.1063/1.1883143]

I. INTRODUCTION

Alkali niobates, such as $LiNbO_3, NaNbO_3$, and $KNbO_3$ have received much attention due to their interesting ferroelectric or antiferroelectric phase transitions and their technical applications. For example, $LiNbO_3$ has a ferroelectric phase transition at 1200 °C. At room temperature it possesses an attractive combination of piezoelectric and electro-optic properties, which enable it to be widely used in nonlinear optics, optoelectronics, and acoustics. Several phase transitions take place in $KNbO_3$ including two ferroelectric–ferroelectric and one ferroelectric–paraelectric transitions. Its room temperature ferroelectric phase has the largest nonlinear optical coefficient among all commercially available inorganic materials, so it is normally used for frequency doubling of low and medium power lasers. Recently, another alkali niobate $Cs_2Nb_4O_{11}$(CNO) was found to have a ferroelectric-like phase transition at 164 °C. Kharitonova *et al.* grew the single crystal of CNO and measured its dielectric constant and second harmonic generation (SHG) at high temperature up to 600 °C.[1] They found that the dielectric constant of the single crystal showed no anomalies along the crystal *a* and *b* axes, but exhibited a sharp λ-shaped peak along *c* axis with a maximal value of about 4800 at 164 °C, above which the dielectric constant follows the Curie–Weiss law. They also observed an anomaly in SHG at the same temperature that SHG slightly decreased and persisted above

164 °C up to 380 °C. In addition, they found temperature hysteresis of the anomalies was lacking or very small, so they deduced the transition associated with the anomalies was of the second order. For the purpose of studying this newly discovered potential ferroelectric material and exploring its technical application, we carry out a thorough study of its electrical properties, vibrational spectra, and the mechanism of the phase transition.

CNO was first obtained by Reisman and Mineo in the $Cs_2O–Nb_2O_5$ system.[2] At room temperature CNO was reported to have an orthorhombic structure[3] with space group *Pnn*2 (The conventional space group setting *Pnn*2 is used in this article instead of *P*2*nn* as in Ref. 3). There are eight chemical formula units in a unit cell. The unit cell parameters are $a=7.464$ Å, $b=28.898$ Å, and $c=10.484$ Å. Figure 1 illustrates its crystal structure that contains NbO_6 octahedra and NbO_4 tetrahedra being linked together to form a three-dimensional framework with Cs atoms located inside interlinked channels.

Impedance and Raman spectroscopy are powerful experimental techniques used to study electrical properties and structural phase transitions in solids. We have studied the phase transition, dielectric relaxation, and conduction process in $Bi_2Ti_4O_{11}$,[4] the origin of large dielectric constant in $Bi_{2/3}Cu_3Ti_4O_{12}$,[5] and the phase transition in $Na_{0.5}Bi_{4.5}Ti_4O_{15}$[6] by using these techniques. In this article, we first investigate the temperature and frequency dependence of the complex impedance of CNO at frequency range $10^{-1}–10^6$ Hz and temperature range 30–300 °C, then mea-

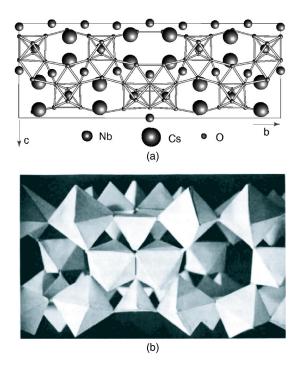a)Electronic mail: jliu@unlserve.unl.edu

FIG. 1. Crystal structure of CNO at room temperature. (a) Projection along a axis. (b) arrangement of NbO_6 octahedra and NbO_4 tetrahedra in the structure (from Ref. 3).

FIG. 2. Temperature dependence of complex capacitance C^* at different frequencies. (a) Real part C', (b) imaginary part C''.

sure the room temperature and high-temperature polarized Raman spectra, from which we observe anomalies at about 165 °C and identify them as an indication of a phase transition. Using the pseudosymmetry analysis, we infer this phase transition as a structural change from the room temperature orthorhombic $Pnn2$ to another orthorhombic $Imm2$.

In Sec. II, we describe experimental methods, such as crystal growth, sample preparation, and impedance and Raman measurement. Then, in Sec. III, we present the experimental results and discussions. First, we report the temperature and frequency dependence of the complex capacitance and impedance. Second, we present the polarized Raman spectra at room and high temperatures. Third, we elucidate the mechanism of the structural phase transition based on the pseudosymmetry analysis. Finally, we present the conclusion in Sec. IV.

II. EXPERIMENT

A CNO single crystal was grown by flux method from melt of binary $Cs_2O-Nb_2O_5$ system with spontaneous nucleation. $CsNO_3$ and Nb_2O_5 were used as starting materials. The best result was obtained with use of the melt containing 47 mol % $Cs_2O(CsNO_3)$ and 53 mol % Nb_2O_5. The mixture of the above components was first heated to 600 °C, then was mixed again, placed in a 50 ml platinum crucible and heated at 1150 °C for 12 h and cooled at the rates of 0.3 °C/h to 1090 °C. After that, the melt was poured out and crystals were cooled to room temperature and washed in warm water to remove traces of solvent. The chosen crystal was cut to a size of $2.08 \times 4.82 \times 2.12$ mm^3 perpendicular to the crystal a, b, and c axes with the c axis parallel to the twofold axis
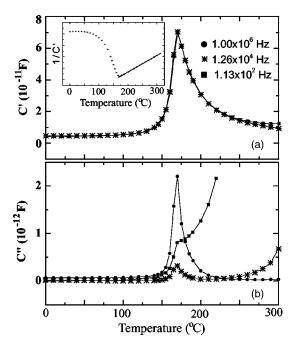
and the a and b axes parallel to each of the two glide planes of the crystal. After optically polishing the crystal became colorless and transparent.

Complex impedance Z^* was measured by using a Novocontrol alpha high-resolution dielectric analyzer in the temperature range 30–300 °C and the frequency range $10^{-1}-10^6$ Hz. Silver films were vaporized on both faces normal to the c axis as electrodes. The ac field was applied along the c axis and the voltage was 1 V.

Z^* was obtained in the usual way, i.e., $Z^* = Z' - iZ'' = V^*/I^*$, where V^* and I^* are the applied voltage and resulting current, respectively. Then complex capacitance C^* was calculated as following:

$$C^* = C' - iC'' = \frac{1}{i\omega Z^*}. \tag{1}$$

In Raman measurement, incident light was provided by 514.5 nm radiation of a Spectra-Physics argon ion laser operating with an output 200 mW. Scattered light was recorded by a SPEX 1401 double monochromator with scattering configurations $y(zz)x, y(xy)x, z(xz)y$ and $z(yz)x$ which correspond to $A_1(TO), A_2, B_1(TO)$, and $B_2(TO)$ modes, where the first and fourth letters in the scattering configurations represent directions of the incident and scattered light, respectively, while the second and third letters are their polarized direction; besides, A_1, A_2, B_1, and B_2 are symmetry species or irreducible representations of point group $C_{2v}(mm2)$, and TO represents a transverse optical mode.

III. RESULTS AND DISCUSSION

A. Impedance study

In Fig. 2 we present temperature dependence of the complex capacitance C^* along the crystal c axis at three different frequencies (113, 1.26×10^4, and 1×10^6 Hz). We observed a
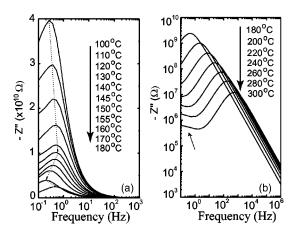
FIG. 3. Frequency dependence of imaginary part Z'' of impedance Z^* at different temperatures.

strong λ-shaped peak at 165 °C in real part C' as shown in Fig. 2(a) whose shape and maximal value are independent of frequencies. Imaginary part C'' in Fig. 2(b) also shows an anomaly at the same temperature. In addition, C'' increases rapidly above 165 °C at frequency 113 Hz due to the increase of conductivity. The anomalies in C' and C'' indicate the crystal undergoes a phase transition at 165 °C. Above the phase transition C' follows the Curie–Weiss law $1/C' = (1/C_0)(T-T_0)$ as shown by the inset in Fig. 2(a), where C_0 is the Curie–Weiss constant, and T_0 the Curie–Weiss temperature.

Figure 3 depicts frequency dependence of imaginary parts (Z'') of the complex impedance $Z^* = Z' - iZ''$ along the crystal c axis at different temperatures. At temperatures below 90 °C, only the tail of a strong response peak shows up in the measured frequency range. The maximum of the peak appears above 100 °C. In Fig. 3(a) we observe the peak position of Z'' changes back and forth; namely, it first shifts to higher frequency until 145 °C, then moves backward until T_c, from which it shifts to higher frequency again up to the highest temperature of the experiment. During the entire process, the intensity of the peak continuously decreases. Moreover, we notice that in Fig. 3(b) low-frequency end of the peak starts to rise at 240 °C and above, indicating that another response peak begins to emerge.

For a single crystal, its electrical response often contains contributions from both bulk and electrode effects. Since the electrode effect is characterized by a larger relaxation time than the bulk response, two separate peaks are usually observed in the $Z'' \sim f$ plots.[7] As we can see below that the peaks shown in Figs. 3 result from the bulk response whose associated capacitance shows a sharp peak at T_c, while the emerging peak at the low-frequency side above 240 °C [indicated by the short arrow in Fig. 3(b)] is related to the electrode effect.

To analyze the impedance spectra, data usually are modeled by an ideal equivalent circuit consisting of a resistor R and capacitor C.[8] When two electrical response mechanisms are involved, electrical properties of the system are represented by the equivalent circuit shown in Fig. 4, which consists of a series array of two sub-circuits, one represents bulk response and the other for the electrode effect. Each sub-
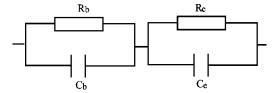

FIG. 4. Equivalent circuit used to represent the electrical properties of bulk and electrode polarization effects.

circuit is composed of a resistor and capacitor joined in parallel. Let (R_b, R_e) and (C_b, C_e) be the resistances and capacitances of bulk and electrode effects, respectively, then the impedance Z^* for the equivalent circuit is

$$Z^* = \frac{R_b}{1 + i\omega R_b C_b} + \frac{R_e}{1 + i\omega R_e C_e}. \qquad (2)$$

As shown in Fig. 3, the electrode effect has rather minor influence on the response peak of the bulk effect. Since we are only interested in the bulk effect, so we neglect the electrode effect and fit our observed data by using the following equation:

$$Z^* = \frac{R_b}{1 + i\omega R_b C_b} = \frac{R_b}{1 + (\omega \tau_b)^2} - i\frac{R_b \omega \tau_b}{1 + (\omega \tau_b)^2}, \qquad (3)$$

where $\tau_b = R_b C_b$ is the relaxation time of the bulk effect. The fitted results at different temperature are presented in Fig. 5 as solid curves. We noticed that at temperatures below 200 °C, the bulk response can be described by an ideal Debye relaxation; when the temperature increases to 250 °C, the observed values start to deviate from the fitted curve on the low-frequency side due to the emergence of the electrode contribution.

In addition, from fitting the data we obtain the bulk resistance R_b, capacitance C_b and calculated relaxation time $\tau_b = R_b C_b$ at different temperatures, which are plotted in Fig. 6. We can see that the bulk resistance R_b decreases with increasing temperature over the entire measured temperature range [Fig. 6(a)], while the bulk capacitance C_b exhibits a λ-shaped peak [Fig. 6(b)] exactly like the behavior obtained from the direct measurement shown in Fig. 2(a). Regarding the relaxation time $\tau_b = R_b C_b$, it slowly decreases with in-
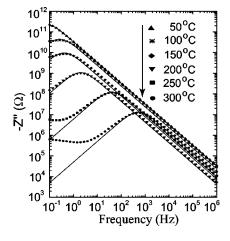

FIG. 5. Frequency dependence of imaginary part Z'' of impedance Z^* at different temperatures. Solid lines represent fitted results.
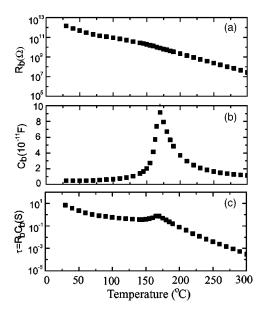
FIG. 6. Temperature dependence of fitted parameters. (a) Bulk resistance R_b, (b) bulk capacitance C_b, (c) relaxation time $\tau_b = R_b C_b$.

FIG. 7. Room temperature Raman spectra in different symmetries of normal vibrations.

creasing temperature from 30 to 145 °C, then increases and shows a bump at T_c [Fig. 6(c)]. From Eq. (3) we know that τ_b determines the response peak frequency $f_{\max} = 1/(2\pi\tau_b)$, namely, the peak shifts to higher frequency as τ_b decreases; it moves back when τ_b increases; thus the temperature dependence of τ_b shown in Fig. 6(c) explains the shifting behavior of response peak shown in Fig. 3(a).

B. Raman scattering study

1. Group theory analysis of lattice vibrations

At room temperature the space group of CNO is orthorhombic $Pnn2$.[3] Since there are eight chemical formula units in a unit cell, a total of 408 normal modes of vibrations are expected for the CNO crystal. Based on the nuclear site group analysis,[9] irreducible representations of the 408 lattice vibrations in the center of Brillouin zone may be classified as following:

$$\Gamma_{Pnn2} = 101A_1 + 101A_2 + 103B_1 + 103B_2, \qquad (4)$$

where $A_1 + B_1 + B_2$ are three acoustic modes, $100A_1 + 101A_2 + 102B_1 + 102B_2$ are optical modes, all of which are Raman active, and $A_1, B_1,$ and B_2 are also infrared active. The Raman scattering tensors are[10]

$$A_1(z) \sim \begin{pmatrix} a & 0 & 0 \\ 0 & b & 0 \\ 0 & 0 & c \end{pmatrix}, \quad A_2 \sim \begin{pmatrix} 0 & d & 0 \\ d & 0 & 0 \\ 0 & 0 & 0 \end{pmatrix},$$

$$B_1(x) \sim \begin{pmatrix} 0 & 0 & e \\ 0 & 0 & 0 \\ e & 0 & 0 \end{pmatrix}, \quad B_2(y) \sim \begin{pmatrix} 0 & 0 & 0 \\ 0 & 0 & f \\ 0 & f & 0 \end{pmatrix}, \qquad (5)$$

where $a, b, c, d, e,$ and f in the matrices represent the nonvanishing components of the Raman tensors, and an x, y, z in brackets indicates the polarization direction of infrared active mode.
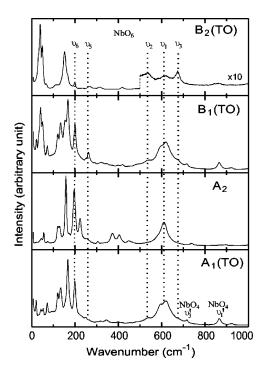
2. Polarized Raman spectra at room temperature and mode assignments

Room temperature polarized Raman spectra of CNO are shown in Fig. 7, which are similar to those of niobates that contain NbO_6 octahedron ions such as $LiNbO_3$,[11] and $BiNbO_4$.[12] The number of observed Raman modes is much smaller than predicted by group theory. The wavenumbers of all observed Raman bands are presented in Table I.

As shown in Fig. 1, the crystal structure of CNO consists of deformed NbO_6 octahedra and NbO_4 tetrahedra interlinked by corner-sharing or by edge-sharing. These octahedra and tetrahedra build up a three-dimensional network with channels in which the Cs atoms are located. It is well-known that in metal oxides with octahedral or tetrahedral coordination, the intragroup binding energy within the octahedron or tetrahedron is larger than the intergroup or crystal binding energy. Therefore, to the first-order approximation, we can think that the vibrational spectra of CNO are primarily composed of internal vibrations of NbO_6 octahedra and NbO_4 tetrahedra, together external vibrations of the lattices which occur at lower frequencies and arise from cation-octahedra–tetrahedra and intergroup librations.

Isolated NbO_6 octahedron has the symmetry of point group O_h and 15 internal vibrational degrees of freedom. From group theory analysis its six normal vibrational modes can be represented as

$$\Gamma_{\text{oct}} = A_{1g}(\nu_1) + E_g(\nu_2) + 2T_{1u}(\nu_3, \nu_4) + T_{2g}(\nu_5) + T_{2u}(\nu_6), \qquad (6)$$

where $A_{1g}, E_g, T_{1u}, T_{2g},$ and T_{2u} are the irreducible representations of the point group O_h, $\nu_1, \nu_2,$ and ν_5 are Raman active, ν_3, ν_4 infrared active, and ν_6 silent. Among them ν_1, ν_2 are pure stretching vibrations of Nb–O bonds, ν_5 and ν_6 are

TABLE I. Wavenumbers (unit: cm^{-1}) of the Raman modes and assignments to the internal vibrations of the NbO$_6$ octahedra and the NbO$_4$ tetrahedra (s=strong, m=medium, w=weak, br=broad, sh=shoulder, v=very).

$A_1(TO)$	A_2	$B_1(TO)$	$B_2(TO)$	Assignment
21s		22m	31s (sh)	
		33s(sh)	39vs	
43m	45w	41vs	49vs	
53m	56m	50vs		
72s	75vw	72m	69vw	external modes
120s	121m	121s	110vw (br)	
134s	128m	134s		
	158vs	155s	152s	
166vs		167vs	166s (sh)	
199vs	197vs	200s	199m	ν_6-NbO$_6$
	224s			ν_6-NbO$_6$
250vw	253vw(sh)		234vw	ν_5-NbO$_6$
268vw	265vw(sh)	262m	266w	ν_5-NbO$_6$
304vw	306vw		313w	ν_4-NbO$_6$
319vw		323vw	318w	ν_4-NbO$_6$
345w		346vw		
399vw (br)	374m	398vw		
	404m	419vw		
	449w			$\nu_4'-$NbO$_4$
541w (br)		542w (sh)	536vw	ν_2-NbO$_6$
597s		600s		ν_1-NbO$_6$
620s	611s	621s	620vw	ν_1-NbO$_6$
		671w(sh)	675vw	ν_3-NbO$_6$
716w	737w	716vw		$\nu_1'-$NbO$_4$
866m	868vw	865vw	864vw	$\nu_3'-$NbO$_4$
923w		921vw	922vw	

interbond angle bending vibrations between Nb–O bonds, and ν_3 and ν_4 are considered as combinations of stretching and bending. Since the NbO$_6$ octahedra in CNO are highly distorted, we anticipate all its normal modes become Raman active and show up in the Raman spectra.

Based on the Raman peak assignments of LiNbO$_3$,[13] and BiNbO$_4$,[12] we can identify the internal vibrations of NbO$_6$ octahedron in the observed Raman spectra of CNO shown in Fig. 7: The strong band at about 600 cm^{-1} is the symmetric stretching mode ν_1 of NbO$_6$ octahedron, which splits into two peaks in $A_1(TO)$ and $B_1(TO)$; left shoulder of the ν_1 mode at around 541 cm^{-1} originates from ν_2, whereas the peak at 675 cm^{-1} in $B_2(TO)$ and right shoulder of the ν_1 in $B_1(TO)$ belong to the ν_3 mode, which appears at 680 cm^{-1} in LiNbO$_3$ crystal;[13] since mode ν_4 usually occurs in the range 300–400 cm^{-1}, so the peaks in this region should originate from the ν_4 mode; the peak at about 268 cm^{-1} is assigned to the ν_5 mode; it is stronger in the $B_1(TO)$ than in other symmetries; finally, the Raman band at 199 cm^{-1} is due to the ν_6 mode, which occurs at the same position in BiNbO$_4$.[12]

Isolated NbO$_4$ tetrahedra has the symmetry of point group T_d. Its four normal vibrations are

$$\Gamma_{\text{tetra}} = A_{1g}(\nu_1') + E(\nu_2') + 2T_2(\nu_3', \nu_4'), \qquad (7)$$

where A_{1g}, E, and T_2 are the irreducible representations of point group T_d, all of them are Raman active, while $T_2(\nu_3', \nu_4')$ is also infrared active. Thus they are all expected to show up in the Raman spectra of CNO.

Since Nb atom is usually too large to squeeze into an oxygen tetrahedron, only a few rare-earth ANbO$_3$ (A=Sm, La, Y, Yb) compounds were reported to have NbO$_4$ units, among them, YNbO$_3$ and YbNbO$_3$ were investigated by Raman scattering.[14,15] Based on the experimental Raman data of YNbO$_3$, Blasse[14] deduced that the vibrational modes of a regular NbO$_4$ tetrahedron with no interactions and distortions occur at $816(\nu_1'), 650(\nu_3'), 420(\nu_4')$, and $340 (\nu_2')$ cm^{-1}. These modes were observed by Jehng and Wachs[15] at about 813, 717, 435, and 331 cm^{-1}, respectively, in the Raman spectra of YbNbO$_3$. Comparing with them, we assign the peak at 866 cm^{-1} in Fig. 7 to the ν_1' mode of NbO$_4$ tetrahedra, band at 716 cm^{-1} to the ν_3' mode, and band at 449 cm^{-1} in A_2 symmetry to the ν_4' mode. Since ν_2' mode appears in the same region as ν_4 mode of NbO$_6$ octahedron, it cannot be assigned unambiguously.

Raman bands below 170 cm^{-1} belong to the external vibrations of the crystal, which originate from the translational vibrations of the Cs atoms and librational vibrations of NbO$_6$ octahedra and NbO$_4$ tetrahedra, and can not be clearly assigned.

3. Polarized Raman spectra at high temperature

Figure 8 exhibits the temperature dependence of $A_1(TO)$ modes recorded in the $y(zz)x$ configuration. Abrupt decrease of intensity, broadening of linewidth, and disappearance of some peaks above 170 °C give a clear indication of a phase
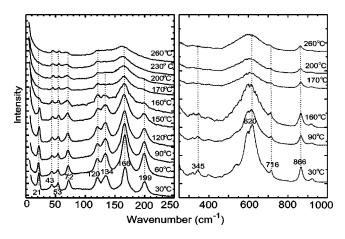
FIG. 8. High temperature Raman spectra with $A_1(TO)$ symmetry.

transition occurring between 160 and 170 °C, which is consistent with the anomaly in the complex capacitance at 165 °C shown in Fig. 2(a).

From Fig. 8, we observed a general decrease in intensity and increase in linewidth as the temperature increases. However, the changes are drastic at the phase transition temperature T_c. Raman peaks at 21, 134, 199 cm^{-1}, and the small peaks around 345 cm^{-1} vanish above T_c. Bands at 72, 120, and 166 cm^{-1} persist to the high-temperature phase but become very broad. The stretching modes ν_1 and ν_2 of NbO$_6$ octahedron at 600 and 541 cm^{-1} merge into a broad band. We also noticed that the positions of most Raman bands hardly depend on the temperature except bands at 43 and 53 cm^{-1} which slightly shift to higher wavenumbers at high temperature. The temperature dependence of $B_1(TO)$ and $B_2(TO)$ modes are also similar to those of $A_1(TO)$ modes described above.

C. Phase transition mechanism

We noticed the following important features by summarizing the experimental results. First, the temperature dependencies of complex capacitance and Raman spectra both showed that there is a phase transition at 165 °C in CNO. Second, our sample maintained its integrity and perfect optical transparency after passing through T_c several times. Finally, it was reported that temperature hysteresis of the phase transition was lacking or very small.[1] Therefore, we deduce that this 165 °C phase transition in CNO does not involve structural reconstruction, but is caused by small displacive distortions between two structures, usually referred as displacive or Landau-type transition, in which the low and high symmetry structures are connected by a group-supergroup relationship.[16]

Mechanism of structural phase transition in crystals is often studied experimentally by determining crystal structures both below and above T_c. However, group-theoretical methods are also very effective and widely used. For example, Stokes and Hatch developed a technique that starting from a high-symmetry structure, all possible low-symmetry structures after a Landau-type phase transition can be deduced from isotropy subgroup decomposition.[17] Contrast to this technique, Igartua *et al.* developed a pseudosymmetry

analysis approach by which high-symmetry structure can be predicted based on a low-symmetry structure.[18,19] In the pseudosymmetry analysis, when the atomic coordinates of a given structure display an approximate symmetry in addition to the actual space-group symmetry, the structure can be considered as pseudosymmetric with respect to a supergroup containing this additional symmetry, thus the structural pseudosymmetry can be interpreted as the result of a distortion from prototype structure with higher symmetry.[18,19] If the distortion is small enough, it is probable that the system acquires this more symmetrical configuration at higher temperatures through a Landau-type structural phase transition.[16] Accordingly, in order to find materials with a structural phase transition at high temperature, one must look for substances which have such pseudosymmetry. A general procedure for a systematic pseudosymmetry search among structures with a given space group symmetry has been developed.[18,19] It is based on the assumption that the higher approximate symmetry is described by a super-group of the structure space group. As any group-supergroup chain can be represented by a chain of minimal supergroups, the search for pseudosymmetry is restricted to the minimal supergroups of the structure space group. The detailed search procedure has been described in Refs. 18 and 19, and implemented by the program PSEUDO.[20] This procedure has been successfully applied to predict possible high-temperature phase transitions, including ferro-electric transitions, for inorganic structures with space groups $P2_12_12_1$,[18] $Pnma$,[21] $Pba2$,[19] and $Pmc2_1$[19] listed in the inorganic crystal structure database (ICSD). In this work we use the program PSEUDO to investigate the mechanism of the phase transition we observed in CNO. To start, the program requires the space group of the crystal structure, cell parameters, and atomic positions in the asymmetric unit as inputs. Results of the calculations contain the pseudosymmetry supergroup, relations between atoms in the initial and transformed structure, atomic displacements necessary to obtain the supergroup, and ideal atomic positions in the supergroup structure.

Based on the room temperature space group $Pnn2$, lattice parameters, and atomic coordinates of CNO,[3] the search for pseudosymmetry has been performed among all of the minimal supergroups of $Pnn2$. The maximum atomic displacement was restricted to be less than 0.75 Å. Usually, pseudosymmetries corresponding to displacements of less than 0.1 Å were not considered as relevant for possible high-temperature phase transitions; such displacements suggest a doubtful symmetry assignment in the structure determination.[19] Of all minimal supergroups of $Pnn2$, we found $Imm2$ was the only possible pseudosymmetric minimal supergroup with the maximum atomic displacement of 0.16 Å. In general, pseudosymmetry search can be continued along the chain of minimal supergroups until no more pseudosymmetry is found.[19] Hence we conducted the search among all minimal super-groups of $Imm2$. We found no pseudosymmetric structure for $Imm2$ with the constraint of maximal atomic displacement less than 0.75 Å. Same result was obtained when relaxing the constraint to 2 Å.

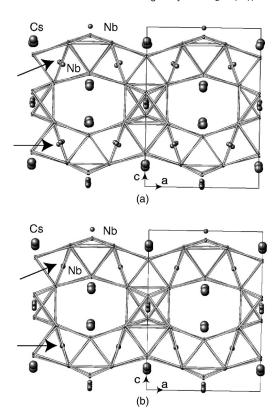Based on the experimental results and deductions from the program PSEUDO, we infer that the phase transition in

FIG. 9. Projections of CNO crystal along the *b* axis. (a) Room temperature *Pnn*2 structure, (b) calculated high temperature *Imm*2 structure. Arrows are used to guide the eyes.

CNO is a structural change from the orthorhombic *Pnn*2 to another orthorhombic *Imm*2. From the isotropy subgroup analysis[17] we know that this phase transition involves the irreducible representation X_2 at the Brillouin zone boundary and the doubling of the primitive unit cell of the *Imm*2 structure. Thus above T_c, some of the Brillouin zone center modes of *Pnn*2 will become zone boundary modes in *Imm*2 and can not be detected by the Raman spectra. In fact, according to the nuclear site group analysis,[9] at the Brillouin zone center of the *Imm*2 structure, CNO would only have 204 normal modes of vibration $\Gamma_{Imm2} = 60A_1 + 41A_2 + 45B_1 + 58B_2$, among them 201 modes are Raman active. Therefore, after the phase transition, among the 405 Raman modes in the *Pnn*2 structure, half of them will vanish. This is in good agreement with our high-temperature Raman measurements, in which we observed several Raman bands disappear above T_c. Ideally we should see a disappearance of exact half modes above T_c in our Raman spectra, but it is impossible to count all Raman bands because many of them are overlapped or too weak to be detected. Moreover, the space group *Imm*2 also has no inversion center, so SHG was found to persist above T_c.[1]

In the *Imm*2 structure, 2 pairs of Nb and 6 pairs of O atoms become symmetry equivalent, all of them displace along three orthorhombic axes of the *Pnn*2 structure, whereas the other atoms that do not become symmetry equivalent only shift along the *a* or *b* axis. From the calculations of the bond lengths and bond angles in *Imm*2, we

found that the octahedra and tetrahedra are much less distorted than those in *Pnn*2. In addition, we present in Fig. 9 the projections along the *b* axis for both the *Pnn*2 and *Imm*2 structures. We noticed that these two structures are quite similar except that the Nb atoms deviate from the centers of octahedra in *Pnn*2 structure, while they are located almost at the centers of octahedra in *Imm*2 structure.

IV. CONCLUSION

We have studied the temperature and frequency dependence of impedance and polarized Raman spectra of single crystal CNO. We found a phase transition at 165 °C indicated by the anomalies of the complex capacitance and Raman spectra. Based on the pseudosymmetry search we proposed this phase transition is originated from a structural change between the room temperature orthorhombic *Pnn*2 and another orthorhombic *Imm*2. We also measured the room temperature Raman spectra in $A_1(TO), A_2, B_1(TO)$, and $B_2(TO)$ symmetries and assigned the high wavenumber Raman bands to the internal vibrations of the NbO₆ octahedra and NbO₄ tetrahedra.

ACKNOWLEDGMENTS

[1]E. P. Kharitonova, V. I. Voronkova, V. K. Yanovskii, and S. Yu. Stefanovich, J. Cryst. Growth, **237–239**, 703 (2002).
[2]A. Reisman and J. Mineo, J. Phys. Chem. **65**, 996 (1961).
[3]Par Madeleine Gasperin, Acta Crystallogr., Sect. B: Struct. Crystallogr. Cryst. Chem. **37**, 641 (1981).
[4]Jianjun Liu, Chun-Gang Duan, Wei-Guo Yin, W. N. Mei, R. W. Smith, and J. R. Hardy, J. Chem. Phys. **119**, 2812 (2003).
[5]Jianjun Liu, Chun-Gang Duan, Wei-Guo Yin, W. N. Mei, R. W. Smith, and J. R. Hardy, Phys. Rev. B **70**, 144106 (2004).
[6]Jianjun Liu, Guangtian Zou, and Yanrong Jin, J. Phys. Chem. Solids **57**, 1653 (1996).
[7]A. K. Jonscher, *Dielectric Relaxation in Solids* (Chelsea Dielectric Press, London, 1983).
[8]J. Ross Macdonald, *Impedance spectroscopy* (Wiley, New York, 1987).
[9]D. L. Rousseau, R. P. Bauman, and S. P. S. Porto, J. Raman Spectrosc. **10**, 253 (1981).
[10]R. Loudon, Adv. Phys. **13**, 423 (1964).
[11]R. F. Schaufele and M. J. Weber, Phys. Rev. **152**, 705 (1966).
[12]Pushan Ayyub, M. S. Multani, V. R. Palkar, and R. Vijayaraghavan, Phys. Rev. B **34**, 8137 (1986).
[13]S. D. Ross, J. Phys. C **3**, 1785 (1970).
[14]G. Blasse, J. Solid State Chem. **7**, 169 (1973).
[15]Jih-Mirn Jehng and Israel E. Wachs, Chem. Mater. **3**, 100 (1991).
[16]P. Toledano and J. C. Toledano, Phys. Rev. B **16**, 386 (1977).
[17]Harold T. Stokes and Dorian M. Hatch, *Isotropy subgroups of the 230 crystallographic space groups* (World Scientific, New Jersey, 1988).
[18]J. M. Igartua, M. I. Aroyo, and J. M. Perez-Mato, Phys. Rev. B **54**, 12744 (1996).
[19]E. Kroumova, M. I. Aroyo, and J. M. Perez-Mato, Acta Crystallogr., Sect. B: Struct. Sci. **B58**, 921 (2002).
[20]E. Kroumova, M. I. Aroyo, J. M. Perez-Mato, S. Ivantchev, J. M. Igartua, and H. Wondratschek, J. Appl. Crystallogr. **34**, 783 (2001).
[21]J. M. Igartua, M. I. Aroyo, E. Kroumova, and J. M. Perez-Mato, Acta Crystallogr., Sect. B: Struct. Sci. **B55**, 177 (1999).